**Atmospheric
Measurement
Techniques
Discussions**

An automated system for selective and continuous measurements of vertical Thoron profiles for the determination of transport times near the ground

D. Plake and I. Trebs

Max Planck Institute for Chemistry, Biogeochemistry Department, P. O. Box 3060, 55020 Mainz, Germany

Correspondence to: D. Plake (daniel.plake@mpic.de)

Abstract

The quantification of in-canopy transport times is of a major importance for the investigation of sources, sinks and net fluxes of reactive trace gases within plant canopies. The Damköhler number, which compares timescales of chemical reactions with transport times, is a widely applied measure to evaluate flux divergences. In this study, we present and evaluate a novel automated measurement system for selective vertical Thoron (Tn) profiles near the earth's surface and demonstrate its suitability for the direct and reliable determination of transport times within a natural grassland canopy. For the first time, we perform a rigorous determination of systematic and random uncertainties of Tn (and Rn) concentrations under field conditions for this type of measurement system. The obtained median precisions for three concentration classes ($> 100\,\mathrm{Bq\,m^{-3}}$, 100–$15\,\mathrm{Bq\,m^{-3}}$, $< 15\,\mathrm{Bq\,m^{-3}}$) were 8.8 %, 23.2 % and 132.1 % for Tn (and 16.6 %, 25.0 %, 99.2 % for Rn). We calculate in-canopy transport times (τ) and propagate it's uncertainty from the individual errors of the Tn concentration measurements. A quality assessment of τ for the field experiment revealed a good data quality with 44 % of the relative uncertainties below 50 %. The occurrence of transport time uncertainties higher than 100 % was caused by absolute Tn gradients lower than $70\,\mathrm{Bq\,m^{-3}\,m^{-1}}$, which was found for 22 % of all determined transport times. In addition, the method was found to be highly sensitive to the Tn concentrations at the upper of two inlet heights (z_u). Low values of $C_{\mathrm{Tn}_{z_\mathrm{u}}}$ result in high absolute uncertainties of the transport time. A comparison of the measured τ with empirical parameterizations revealed the lowest scatter for the measured τ values. We found an excellent agreement of τ with transport times obtained by the in-canopy resistance approach used, e.g. in the SURFATM model during daytime, while the SURFATM model significantly overestimated transport times during nighttime.

1   Introduction

The two isotopes of the radioactive noble gas radon, namely ^{220}Rn (thoron) and ^{222}Rn (radon) and are generated in rocks and natural soils, where the mother nuclides thorium (^{232}Th) and uranium (^{238}U) occur as most common radioactive atoms. Thoron
5 (Tn) and radon (Rn) can migrate into the atmosphere if the location of the production is close enough to the soil-atmosphere interface. The half-life times ($T_{0.5}$) are 55.6 s for Tn and 3.8 d for Rn (Lide, 2004), and limit the transport distances within the soil and the atmosphere. Above the soil the Tn and Rn atoms undergo dilution and transport in atmospheric air until they are removed by radioactive decay, which is their only removal
10 process. Tn and Rn concentrations therefore always decrease with height. Due to its relatively long $T_{0.5}$, Rn is widely used as tracer for regional and global atmospheric transport (cf. Dorr et al., 1983; Zahorowski et al., 2004) and in global circulation models (cf. Brost and Chatfield, 1989; Zhang et al., 2008). In contrast, Tn is excellent for studying meteorological processes in the lowest decametres above soil (Israel, 1965).
15   Soil is to a large extent covered by plant canopies, such as forest, crop or natural grassland, which are sources and sinks of reactive trace gases. Canopies strongly influence the vertical wind profile and other micrometeorological parameters, which drive the trace gas exchange (cf. Finnigan, 2000). The first meter above soil is of significant importance for the surface-atmosphere exchange fluxes of trace gases, since
20 the eddy diffusivity (K) changes by three orders of magnitude (cf. Ikebe and Shimo, 1972), and the transition from turbulent to diffusive transport occurs. The transport time of the air within this layer determines the effectiveness of (a) chemical reactions and inter-conversion of reactive trace gases (termed "chemical flux divergence"; Dearellano et al., 1993) and (b) the deposition and uptake to/by plants and soil of either the directly
25 emitted compounds or their reaction products. For instance, due to long in-canopy transport times only a fraction of soil biogenic nitric oxide (NO) emissions may leave a canopy, because a large part is oxidized by ozone (O_3) and the product nitrogen dioxide (NO_2) is subsequently recaptured mainly through uptake by soil and plant stomata

("canopy reduction") (e.g. Yienger and Levy, 1995). The calculation of Damköhler numbers, which compares chemical timescales to transport times (τ), is a widely applied approach to evaluate the influence of chemistry on exchange fluxes (e.g. Dlugi et al., 2010). Typically, τ or K may be derived using micrometeorological techniques such as the flux-gradient approach. However, their application is limited within plant canopies where, e.g. the Monin-Obukov similarity theory does not hold (Denmead and Bradley, 1985). In addition, practical reasons complicate their in-canopy application (e.g. direct contact of wind sensors and branches).

Rn is mainly used as a tracer in studies focusing on vertical spatial scales of metres to kilometres above soil (e.g. Liu et al., 1984). Some studies present average total flushing times for tall forest canopies (e.g. Trumbore et al., 1990; Ussler et al., 1994; Martens et al., 2004) derived using Rn canopy inventory models (for details see Trumbore et al., 1990). A similar method was used by Simon et al. (2005), who calculated vertical τ profiles for six layers from Rn measurements inside a rainforest canopy.

In contrast, studies dealing with Tn mainly focus on the layer adjacent to the ground, which is due to the competition of transport and the fast radioactive decay. Whereas the Rn decay can be neglected in this part because of the longer $T_{0.5}$. Butterweck et al. (1994) point out that even in a dense canopy, where most micrometeorological methods fail, the turbulent exchange can be characterized with the help of Tn. Consistently, Lehmann et al. (1999) describe the characteristic vertical range for Tn ($z^* = (K/\lambda)^{1/2}$) to be 28 cm (where $\lambda = \ln 2/T_{0.5} = 0.0125\,\text{s}^{-1}$ is the radioactive decay rate (Hänsel and Neumann, 1995) and $K = 10^{-3}\,\text{m}^2\,\text{s}^{-1}$). Furthermore, they propose a straightforward method to determine effective transport times from vertical Tn profiles near the ground as:

$$\tau = \ln\left[\frac{C_{\text{Tn}_{z_l}}}{C_{\text{Tn}_{z_u}}}\right] / \lambda \tag{1}$$

where $C_{\text{Tn}_{z_l}}$ and $C_{\text{Tn}_{z_u}}$ are the measured Tn concentrations at the lower and upper heights (z_l and z_u). These authors call this approach a perfect tool for studying near-

surface gas transport, independently of any particular transport model. The required physical information is entirely provided by the "Tn clock".

The major limitation of Lehmann's method is the precision of the Tn measurement, which was not investigated under field conditions. Two Tn and Rn monitors (Alph-aGuard, Saphymo, Massy, France) were operated in series. Since one AlphaGuard analyser measures the sum of Tn and Rn, the isotope separation is made by applying a defined Tn decay volume, which is installed between the two AlphaGuards. The Tn concentration is then obtained by subtraction of the Rn signal (2nd AlphaGuard) from the sum of Tn and Rn (1st AlphaGuard). Gut et al. (2002), Hens (2009) and Nemitz et al. (2009) applied the same technical setup above a rain forest floor, above a spruce forest floor and within a grassland canopy, respectively. However, none of these studies include a determination of systematic errors between the two AlphaGuards, nor do they estimate random concentration errors. Consequently, the uncertainties of the derived τ values in Lehmann et al. (1999), Hens (2009) and Nemitz et al. (2009) are not determined. In addition, the three measurement heights of the profile in these studies were sequentially switched (time resolution: 10 min sampling per hour and height). Thus, the vertical concentration profiles may be prone to instationarities.

In this paper, we present a novel automated system for selective Tn and Rn profile measurements consisting of three Tn and Rn monitors. We show measured vertical Tn and Rn concentration profiles within a grassland canopy. The influence of instationarities is minimized by continuous and simultaneous measurements at three heights. For the first time, a rigorous determination of systematic and random uncertainties for Tn and Rn concentrations measured under field conditions is made. Due to the outstanding advantages of using Tn to directly determine τ near the ground (see above), we particularly focus our further analyses on Tn. Transport times are calculated from the vertical Tn concentration profiles and the corresponding random concentration errors are propagated in order to quantify the overall uncertainty of τ. We compare quality assessed τ values with empirical parameterizations used in surface-atmosphere exchange models.

An automated system for selective and continuous measurements

D. Plake and I. Trebs

Title Page

Abstract	Introduction
Conclusions	References
Tables	Figures

◀ | ▶|

◀ | ▶

Back | Close

Full Screen / Esc

Printer-friendly Version

Interactive Discussion

2 Methods

2.1 Radon and thoron monitor

The concentrations of Tn and Rn were measured with three commercially available radon monitors (RAD7, Durridge, Billerica, USA). The RAD7 uses a solid state alpha
5 detector for alpha particle counting and electronic alpha spectrometry for differentiation between Tn and Rn. In the sample air, alpha particles of different electric charges are emitted as Tn and Rn decay products. The alpha radiation is converted in the RAD7 measurement chamber to an electric signal and its energy is determined. The RAD7 records a spectrum of the incoming alpha particle energies over a chosen integration
10 time and can distinguish Rn from Tn, which is very rare for currently available commercial Rn monitors.

The RAD7 was developed for locating Tn and Rn entry points in basements of buildings and monitoring of mining galleries, i.e. environments with high Tn and Rn concentrations. Our RAD7 monitors were modified in order to meet the requirements of
15 continuous profile measurements in a grass land ecosystem, with relatively low Tn and Rn concentrations. The sensitivity was enhanced by using a high gain modification provided by the manufacturer consisting of (a) an increased size of the measurement chambers (0.95 L) and (b) alpha detectors with a larger active surface area. In cases when a fast Tn response is required in a standard operation mode, the RAD7 is run in
20 *Sniff mode* with a nominal on-board pump flow rate of $0.65\,L\,min^{-1}$. This low flow rate promotes the reduction of the Tn signal due to fast Tn decay during transport from the sampling point to the RAD7 measurement chamber. To diminish this effect we used an external pump and a mass flow controller (MFC) and set the flow rate to $2\,L\,min^{-1}$. In addition, precise measurements with a RAD7 require atmospheric pressure conditions
25 and a relative humidity (RH) below 10 % in the measurement chamber.

2.2   System setup and configuration

The automated Tn and Rn profile system (Fig. 1) consists of three identical inlet tubes. The hardware components are described in detail in Table 1. The inlet prevents the aspiration of rain drops and particles into the system and is made of a funnel and
5 a membrane filter (Fig. 2a). Sensitive electronic parts like the RAD7s, pumps, MFCs and data recording units are installed in a rack (Fig. 2b) and protected by a water-proof housing. The air is drawn through PFA tubing ($L = 6$ m) from the inlets to the RAD7 monitors in the housing. The tubing is heated above ambient temperature and isolated to avoid condensation of water vapour. In-tubing pressures are permanently
10 monitored upstream of the pumps (see Fig. 1). To achieve the required low RH in the RAD7 monitors, Nafion dryers are installed between pumps and MFCs and are operated at high-pressure. Three Nafion dryers are used in parallel for each inlet height. Downstream of the MFCs atmospheric pressure conditions are achieved by using an open bleed line. The drying purge for the Nafions is operated using the highly efficient
15 reflux method. Hence, a part of the previously dried RAD7 exhaust is flushed counter flow back into the under pressurized drying purge (see Fig. 1). The pressure difference between the sample flow/Nafion and the drying purge is about 2000 hPa.

The RAD7 contains an on-board data logger and a RS232 interface. Data are downloaded using the manufacturer software *Capture* on demand. A home-built V25 mi-
20 croprocessor unit collects e.g. the data from the pressure sensors of the Tn and Rn profile system and from a vertical thermocouple profile (ASPTC, Campbell Scientific, Utah, USA). A specially programmed Labview software running on a master-PC requests every 10 s the data from the V25 via RS232 connection. The MFC flow rates are monitored periodically with the Labview software.

25   2.3   Application in the field

The field measurements to test and validate the system were made from July to September 2011 in Rhine Hessen (Germany) at the estate of the Mainz Finthen Airport

Title Page

Abstract Introduction

Conclusions References

Tables Figures

◄ ►

◄ ►

Back Close

Full Screen / Esc

Printer-friendly Version

Interactive Discussion

(49.9685° N, 8.1481° E). The vegetation type is classified as a nutrient poor steppe-like grassland ecosystem with a mean canopy height of 0.6 m. A continuous Tn and Rn profile data set of 51 days is available (6 August–25 September 2011). The integration time of the RAD7 monitors was set to 60 min. The vertical wind speed profile was measured at heights of 0.2 m, 0.8 m, 1.5 m, 2.5 m, 4.0 m (2-D ultra sonic anemometer, WS425, Vaisala, Finland). In addition, the three dimensional wind vector and temperature were measured at 20 Hz by a sonic anemometer (CSAT-3, Campbell Scientific) located at 3.0 m above ground and recorded using a data logger (CR3000, Campbell Scientific). The friction velocity (u_*), sensible heat flux (H) and stability parameters were calculated using the Eddy-Covariance Software TK3 (see Mauder and Foken, 2011).

The arrangement of the inlet heights was varied throughout the field experiment (Fig. 3). Although, the vertical inlet separation should be maximal in order to increase the observed vertical concentration differences, for Tn this approach is restricted due to its short $T_{0.5}$. A more compact inlet arrangement close to the soil (e.g. Fig. 3, block 2) might be favoured since all Tn may nearly be decayed just above the canopy.

2.4 System characterization

2.4.1 Tn decay versus system residence time

Due to the short half-life time of Tn the radioactive decay during the residence time of the sample air in the system may significantly reduce the initial Tn concentration at the inlet. A major prerequisite for reliable simultaneous Tn profile measurements with more than one analyser is therefore the achievement of identical residence times in all sample lines. A constant flow rate in our setup is maintained by using precise MFCs. Nevertheless, vertical profile measurements can cause inhomogeneous clogging of the membrane filters used in the different sampling heights, which in turn might cause different residence times. To investigate the decrease of the Tn concentration in our system and to characterize the possible effect of filter clogging we pursued with three steps: (i) pressure characterisation with filter clogging simulation by using a needle

valve, (ii) calculation of residence times from measured flow rates and pressures for laboratory and field conditions, (iii) laboratory measurement of in-situ system residence times.

The pressure in our system was measured at six different positions ($p1$–$p6$) indicated in Fig. 1. Initially, pressures were measured at all positions using a clean filter. This procedure was repeated with the filter replaced by a needle valve to simulate two filter clogging states (medium, dirty) in the laboratory. Subsequently the residence time was calculated for the three filter clogging states based on the continuity equation using the specific dimensions of all hardware components (e.g. tubing length and ID), the in-system pressures ($p1$–$p6$) and the volume flow rate at the MFC. In each part of the system the actual volume flow rate was calculated followed by the determination of section specific residence times. The total system residence time was calculated by summing up the individual residence times. The same procedure was applied for the field campaign data set. Based on the pressure characterisation and the sensor at $p3$ time series of in-system pressures ($p1$–$p6$) were calculated for all inlet tubes and converted into residence times.

The system residence time was measured by replacing the RAD7 with a fast response CO_2 analyser (LICOR7000, Licor Biosciences, Lincoln, USA). CO_2 data were recorded in 0.5 s intervals. Upstream of the inlet system a three-way valve was installed, which controlled the flushing of the tubes with either zero air (0 ppm CO_2) or ambient air ($\sim$ 390 ppm CO_2). After flushing the line with zero air for some time, ambient air was sampled for one second, followed by sampling zero air again. The time that has passed between switching to ambient air and the maximum of the recorded CO_2 peak is defined as the residence time with a clean filter.

The results of the calculations of the residence times under laboratory and field conditions and the in-situ measurement were then compared to quantify the decay of Tn in the system and to evaluate the effect of inhomogeneous filter clogging.

2.4.2 Tn sensitivity

The RAD7 monitors were calibrated by the manufacturer only for Rn. A predefined sensitivity was applied for Tn, which is half of the Rn sensitivity. To ensure the accuracy of the Tn measurements we verified the sensitivity before starting the field measurements. The entire measurement system was setup in the thoron progeny chamber (Fig. 2c) of the radon measurement technique group at the Physikalisch-Technische Bundesanstalt (PTB, Braunschweig, Germany). This group at the PTB developed and operates the world's first primary standard for Tn activity concentration in air (Rottger and Honig, 2011). The RAD7 monitors were compared to the reference instrument of the PTB for the concentration range of 0–4300 Bq m^{-3}.

2.4.3 Side-by-side measurements

Side-by-side (sbs) measurements were performed for sixteen days directly after the campaign under field conditions. The main goals were (a) investigation of systematic differences for Tn and Rn between the three RAD7 monitors (accuracy) under realistic conditions and (b) determination of the random concentration errors of the RAD7 monitors (precision). First, the RAD7 monitors were directly flushed (without tubing) with zero air for two days. These measurements were used to calculate the limit of detection (LOD) for the automated Tn and Rn system under field conditions according to the recommendations of Currie (1968). For the sbs measurements, we installed the inlets inside the well-mixed headspace of a dynamic chamber system (volume 0.041 m^3) (Pape et al., 2009) with an adjustable purging rate of ambient air (0–70 L min^{-1}). Two fans guaranteed well-mixed conditions in the chamber. The bottom of the chamber was closed and two bowls with dried soil from the experimental site were placed inside the chamber serving as Tn and Rn source (Fig. 2d). In order to dilute the emitted Tn and Rn with ambient air the chamber purge was adjusted to different flow rates for several days, these were 70 L min^{-1}, 35 L min^{-1} and 5 L min^{-1} for three, four and seven days, respectively. In contrast to other trace gases, such as O_3 and CO_2, the fast decay of Tn

can cause significant concentration differences even at small horizontal distances of only 15 cm at any time of the day. The application of the well mixed dynamic chamber allowed the performance of reliable sbs measurements under field conditions minimizing the effect of horizontal inlet separation.

2.5 Determination of systematic and random concentration errors

The systematic difference between the RAD7 monitors was determined by plotting the concentrations from the sbs measurements against each other and performing a bivariate weighted linear least-squares fitting regression analysis with the Williamson-York method provided in a Microsoft Excel spread sheet by Cantrell (2008). The counting statistics of the RAD7 monitors provided the weighting errors. The RAD7 at height z_1 was defined as the reference instrument and the slope and intercept of the regressions were used to correct for the systematic error. The remaining scatter around the 1 : 1 line is the random error of the concentration difference of two RAD7 monitors ($\sigma\Delta C$) (see Wolff et al., 2010). This error was found to increase with concentration (see below). To quantify the concentration dependence of $\sigma\Delta C$, we plotted the residuals of the corrected fit, binned them, calculated the means and standard deviations of each bin, and made a linear regression (see Wolff et al., 2010). The resulting regression (slope + intercept) was used to calculate $\sigma\Delta C$ as a function of the Tn and Rn concentration. This random error $\sigma\Delta C$ was calculated for the three RAD7s in all six possible combinations by exchanging x and y-axis. Since the air samples at the three heights were measured with RAD7 monitors of identical age and specifications, we assume the random error of each instrument to be the same ($\sigma C_1 = \sigma C_2$). Thus, we calculated an average of $\sigma\Delta C$ for all monitors and computed σC of one concentration measurement required for the error propagation (see below) as:

$$(\sigma\Delta C)^2 = \sigma C_1^2 + \sigma C_2^2 \tag{2}$$

$$\sigma C = \frac{\sigma\Delta C}{\sqrt{2}} \tag{3}$$

2.6 Determination of transport time uncertainties

A measured Tn profile contains information about the average transport time of air molecules between two measurement heights z_l and z_u for the used integration interval. If the difference of the ambient Tn concentrations measured at z_l and z_u can be resolved, the average transport time (s) can be calculated according to Eq. (1). The application of this method is limited by the prevailing ambient Tn concentrations, transport and dilution by atmospheric turbulence, the instrument precision and the instrument sensitivity (LOD).

In order to estimate the uncertainty of the calculated transport times we applied the Gaussian error propagation method (e.g. Taylor, 1997; Staudt et al., 2011).

$$\sigma_\tau^2 = \overbrace{\left(\frac{\partial \tau}{\partial C_{\text{Tn}_{z_l}}} \cdot \sigma C_{\text{Tn}_{z_l}}\right)^2}^{\text{term A}} + \overbrace{\left(\frac{\partial \tau}{\partial C_{\text{Tn}_{z_u}}} \cdot \sigma C_{\text{Tn}_{z_u}}\right)^2}^{\text{term B}} +$$
$$\underbrace{2\left(\frac{\partial \tau}{\partial C_{\text{Tn}_{z_l}}} \cdot \frac{\partial \tau}{\partial C_{\text{Tn}_{z_u}}} \cdot \sigma C_{\text{Tn}_{z_l}} \cdot \sigma C_{\text{Tn}_{z_u}} \cdot r_{(C_{\text{Tn}_{z_l}}, C_{\text{Tn}_{z_u}})}\right)}_{\text{term C}} \tag{4}$$

where $\sigma C_{\text{Tn}_{z_l}}$ and $\sigma C_{\text{Tn}_{z_u}}$ are the respective concentration errors (see Sect. 2.5), and $r_{(C_{\text{Tn}_{z_l}}, C_{\text{Tn}_{z_u}})}$ is the correlation coefficient of the measured Tn concentrations. Term C is included since the measured Tn concentrations are dependent on each other. We calculated $r_{(C_{\text{Tn}_{z_l}}, C_{\text{Tn}_{z_u}})}$ independently for daytime and nighttime as well as for periods with different inlet arrangements (see Sect. 2.3, Fig. 3).

3 Results

3.1 System characterisation

3.1.1 Tn recovery

The measured pressures during the filter clogging simulation are shown in Fig. 4. The
used absolute pressures at $p2$ were 980 hPa, 960 hPa and 920 hPa for the simulated
filter states clean, medium and dirty, respectively. The pressures from $p2$ to $p5$ were
found to be linearly related for the different filter clogging states. This enabled us to
calculate the pressure at the positions $p1$–$p6$ of the system using the reading of the
permanently installed pressure sensor at $p3$ in each sample line (position see Fig. 1).
The calculated corresponding residence times from the filter clogging experiment were
10.7 s, 10.4 s, and 10.1 s for the clean, medium and dirty state, respectively (Fig. 5).
For comparison, the in-situ measured residence time (maximum of the CO_2 peak) was
11.0 s (Fig. 5). In our experiment (regular filter exchange) the median residence time for
each measurement level calculated from the actual volume flows (see Sect. 2.4.1) was
10.4 s (Fig. 5). The results from the filter clogging simulation in the laboratory represent
well the residence times under field conditions. The results imply that nearly 88 % of the
Tn concentration at the inlet were recovered inside the measurement system (Fig. 5).
If we consider the most extreme residence times during the campaign, the maximal
potential Tn difference between the measurement levels was only 0.8 %. Consequently,
the Tn concentration differences due to filter clogging were neglected in the further data
evaluation.

3.1.2 Tn sensitivity

The verification of the sensitivity in the PTB facility revealed that the predefined Tn
sensitivity from the manufacturer was very accurate. The sensitivity of the three RAD7

Title Page

Abstract | Introduction

Conclusions | References

Tables | Figures

|◄ | ►|

◄ | ►

Back | Close

Full Screen / Esc

Printer-friendly Version

Interactive Discussion

showed a deviation from the reference of less than 8 % within the concentration range of $0\,\mathrm{Bq\,m^{-3}}$ to $4300\,\mathrm{Bq\,m^{-3}}$.

3.1.3 Side-by-side measurements

The regulation of the purging rate in the dynamic chamber allowed us to vary the Tn concentration in the chamber (Fig. 6) to obtain a realistic Tn concentration range (0–$300\,\mathrm{Bq\,m^{-3}}$). The highest Tn concentrations were measured with the lowest purging rate. The scatter of the Tn measurements increased with concentration. In contrast, the Rn concentrations could not be adjusted well using the chamber purging rate. Nevertheless, during stable nighttime situations elevated Rn concentrations were recorded.

3.1.4 Limit of detection

The LOD for Tn (LOD_{Tn}) determined under field conditions with a 60 min integration time when purging the instruments with zero air during the sbs measurement varied by ±20 % for the different RAD7 monitors. In contrast, the LOD_{Rn} was comparable for all RAD7s (Table 2). The determined LOD_{Tn} of $18.3\,\mathrm{Bq\,m^{-3}}$ for an integration time of 60 min was three times higher than that of Rn.

3.2 Systematic and random errors

Figure 7 shows an example for the determination of the systematic and random errors. The averaged random error $\sigma\Delta C$ for Tn and Rn were $\sigma\Delta C_{Tn} = 0.10C + 13.2\,\mathrm{Bq\,m^{-3}}$ and $\sigma\Delta C_{Rn} = 0.19C + 9.5\,\mathrm{Bq\,m^{-3}}$, respectively. Hence, the averaged random concentration error σC (Eq. 3) for Tn and Rn used for the Gaussian error propagation to estimate σ_τ were $\sigma C_{Tn} = \frac{0.10C + 13.2\,\mathrm{Bq\,m^{-3}}}{\sqrt{2}}$ and $\sigma C_{Rn} = \frac{0.19C + 9.5\,\mathrm{Bq\,m^{-3}}}{\sqrt{2}}$. Consequently, the Tn and Rn concentrations where $\sigma C/C = 1$ were $10.0\,\mathrm{Bq\,m^{-3}}$ and $7.8\,\mathrm{Bq\,m^{-3}}$, respectively. The obtained median precisions for three concentration classes ($> 100\,\mathrm{Bq\,m^{-3}}$,

100–15 Bq m^{-3}, < 15 Bq m^{-3}) were 8.8 %, 23.2 % and 132.1 % for Tn and 16.6 %, 25.0 %, 99.2 % for Rn, respectively.

3.3 Radon and thoron concentration profiles

The soil at our measurement site is a much stronger source for Tn than for Rn (median of $C_{Rn}/C_{Tn} = 0.07$ at $z_1 = 0.04$ m). To explain our results, we have selected Tn and Rn concentration measurements of two days in block 2 (period 1) and two days in block 3 (period 2) (Fig. 8a–d) with the respective inlet height arrangements (see Sect. 2.3, Fig. 3). Typical diurnal cycles with higher wind speeds during daytime and lower at nighttime were prevailing during both periods (Fig. 8e–f). The diurnal courses of measured Tn and Rn concentrations mirror the variation of the wind speed, with higher Tn and Rn concentrations during nighttime than during daytime. This is a typical pattern, since at night time stable stratification in the air layer above the canopy top is known to inhibit vertical exchange, while during daytime the vertical exchange is driven by the unstable stratification here. Our temperature profile measurements (not presented) reveal the transition from stable to unstable conditions to take place after sunrise at around 06:00 LT (CET), and the transition from unstable to stable condition some hours before sunset (20:00 LT) at around 16:00 to 17:00 LT. Tn concentrations ranged from 0 to 830 Bq m^{-3} and Rn concentrations ranged from 0 to 250 Bq m^{-3}, both with highest concentrations close to the ground.

A pronounced vertical Tn profile was measured during period 1 (Fig. 8a). The measured Tn concentration differences between z_1 and z_3 were about 400 Bq m^{-3} during midnight and about 130 Bq m^{-3} in the early afternoon. These values were typical for period 1 and the precision of the RAD7 monitors was sufficient to resolve significant vertical concentration differences. Obviously, this inlet height arrangement was optimal to determine vertical Tn concentration differences.

In contrast, we found that the inlet arrangement of period 1 was not suitable to measure significant vertical Rn concentration differences between all three heights

(Fig. 8c). In particular, the daytime Rn concentrations at z_2 and z_3 were often within the random concentration error (see Sect. 3.2) and the scatter of the concentrations further complicates the determination of significant Rn differences.

After increasing the inlet separation distance (period 2), the Tn concentration differences between z_1 and z_2 (Fig. 8b) are still significantly different from each other. The concentrations at z_1 and z_2 range from daytime values of $100\,\mathrm{Bq\,m^{-3}}$ and $\sim 20\,\mathrm{Bq\,m^{-3}}$, respectively, to nighttime values of $600\,\mathrm{Bq\,m^{-3}}$ and 100–$300\,\mathrm{Bq\,m^{-3}}$, respectively. However, the Tn concentrations measured at $z_3 = 80\,\mathrm{cm}$ are always below $30\,\mathrm{Bq\,m^{-3}}$ during period 2 and may occasionally reach the $\mathrm{LOD_{Tn}}$.

The Rn nighttime profile (Fig. 8d) shows substantially higher concentration differences (25–$250\,\mathrm{Bq\,m^{-3}}$) than during period 1. With this inlet arrangement the precision of the RAD7 monitors was sufficient to resolve significant vertical Rn concentration differences during nighttime.

The concentrations at z_2 in period 2 are similar to those at z_3 in period 1 since the inlet heights were identical (see Sect. 2.3).

3.4 Calculation of transport times and quality assurance

Since the subject of this paper is the description and evaluation of the novel automated measurement system, we will mainly focus on the data quality, rather than describe and interpret diurnal courses of the transport times. Transport times τ were calculated using the measured Tn concentrations (Fig. 8a, b) using Eq. (1). The propagation of previously determined random concentration errors (σC) enabled us to assign each value of τ with an absolute uncertainty (σ_τ) (see Eq. 4). We assessed the data quality of τ using a classification according to the magnitude of the relative uncertainty. Three data quality classes were introduced ($\frac{\sigma_\tau}{\tau} < 0.5$: good; $0.5 \leq \frac{\sigma_\tau}{\tau} < 1$: adequate; $\frac{\sigma_\tau}{\tau} \geq 1$: inadequate quality).

The calculated transport times for the two investigated periods are shown in Fig. 9. Our setup allowed the calculation of τ for three layers within the canopy. The lower

layer was between z_1 and z_2 (Fig. 9a, b), the upper layer between z_2 and z_3 (Fig. 9c, d) and the overall transport time between z_1 and z_3 (Fig. 9e, f). Due to the varying inlet height arrangements in period 1 and 2 the lower and upper layers were not identical. However, the overall transport time during period 1 (Fig. 9e) corresponds to the one

5 of the lower layer in period 2 (Fig. 9b), representing the transport between 0.04 m and 0.20 m.

During period 1, with its more compact inlet arrangement closer to the ground both τ in the lower and in the upper layer ranged between 20 s and 150 s (Fig. 9a, c). The overall transport time of period 1 (Fig. 9e) corresponds to the sum of both other layers

10 and indeed featured a similar diurnal pattern as in the lower layer during period 2 (Fig. 9b). These values were highest from around 06:00 to 12:00 LT ranging from 200 s to 300 s and were lower during nighttime (50–150 s). The diurnal course of τ in the upper and lower layer during period 2 were rather different from each other (Fig. 9b,d). In the lower layer τ ranged from nighttime minima of 100 s to midday maxima of about

15 300 s. In contrast, the τ values in the upper layer featured maxima during nighttime of up to 350 s and daytime minima ranging from 10 s to 120 s. The overall transport time during period 2 (Fig. 9f) shows the largest values always above 120 s with maxima occasionally exceeding 400 s, which is attributed to the large layer thickness of 0.76 m.

The transport times calculated for period 1 generally show a better data quality than

20 those for period 2 (pie diagrams in Fig. 9). For period 1, 94 %, 88 % and 98 % of the calculated τ values for the lower, upper and overall layer, respectively, are of good data quality. During period 2 the lower and overall layer show a comparably good data quality with 100 % and 94 % of the τ values with good quality, whereas 40 % and 42 % of the τ values in the upper layer are of adequate and inadequate data quality, respectively.

25 Calculated τ values belonging to the inadequate data quality class can be found at any time of the day and stand in many cases out of the general diurnal course (often as extreme values) in the corresponding plots (e.g. Fig. 9c, d and f).

Title Page

Abstract | Introduction

Conclusions | References

Tables | Figures

◀ | ▶

◀ | ▶

Back | Close

Full Screen / Esc

Printer-friendly Version

Interactive Discussion

4 Discussion

4.1 System performance

The presented system for the continuous determination of transport times near the ground is based on vertical Tn profile measurements at three heights using three RAD7 monitors that are selective for Tn and Rn. Although other examples for auto-mated Tn profile measurements can be found in the literature (e.g. Lehmann et al., 1999; Nemitz et al., 2009; Gut et al., 2002; Hens, 2009), the major drawback of these studies is the application of a pair of non-selective monitors to measure a sequentially switched profile. Thus, the measured vertical concentration differences are prone to instationarities, particularly for longer integration times. While their method minimizes systematic errors between the measurement heights, the random error of the Tn con-centration can be amplified since it is determined from the difference of two signals of non-selective monitors (for details see Lehmann et al., 1999). In contrast, the system of Butterweck et al. (1994), who operated a simultaneous profile consisting of four instru-ments that are selective for Tn and Rn, is not prone to instationarities. Nevertheless, none of the previous studies assessed systematic or random errors of the determined Tn concentration profiles and the calculated τ values. Such an analysis is crucial for applications with multiple analysers and required for a thorough interpretation of the in-canopy transport.

The overall performance of the novel automated measurement system was satis-fying, with a Tn recovery of 88 % that was relatively stable and comparable for all sampling lines. Our setup comprising PFA tubing, pumps, Nafion tubing and MFCs strongly modified the standard setup of the RAD7 monitors. The performance of the Nafion dryers was excellent with an average RH of 4 % in all RAD7 throughout the field experiment.

We found that the signal of the RAD7 at low concentrations is quite noisy. The higher LOD for Tn ($18.3\,\mathrm{Bq\,m^{-3}}$) than for Rn was largely caused by the lower sensitivity of the RAD7 for Tn. The Tn instruments used in Butterweck et al. (1994) exhibit an even

higher LOD_{Tn} of $37\,Bq\,m^{-3}$ for the same integration time (Wicke and Porstendorfer, 1983). The LOD_{Tn} for the setup used e.g. in Lehmann et al. (1999) is not mentioned. Since they determine Tn as the sum of two AlphaGuard signals we assume that the LOD_{Tn} also exceeded LOD_{Rn} for their setup.

The determined mean LOD_{Rn} of $6.2\,Bq\,m^{-3}$ (see Table 2) is high compared to that of Wada et al. (2010), who developed an electrostatic Rn system with an LOD_{Rn} between 0.16 and $0.2\,Bq\,m^{-3}$ for 60 min integration time. They achieved this by operating it at a flow rate of $3\,L\,min^{-1}$ and by using much larger measurement chambers of 32 L and 16.8 L volume, respectively. The LOD_{Rn} of the system used in Butterweck et al. (1994) is also comparably small with $1\,Bq\,m^{-3}$ at 60 min integration time (Wicke and Porstendorfer, 1983). In contrast, the LOD_{Rn} of the AlphaGuard operated at 10 min integration time, as used in the studies of Lehmann et al. (1999), Nemitz et al. (2009) and Hens (2009), was determined to be $12\,Bq\,m^{-3}$ by Hens (2009) and, therefore, twice as high as for the RAD7.

Since the RAD7s were not explicitly calibrated for Tn by the manufacturer, we validated the accuracy for Tn in the PTB facility and by sbs measurements under field conditions. The systematic error determined in the PTB of 6 % to 8 % was somewhat higher than the results from the sbs measurements, which were in the order of 1 % to 3 % (compare Fig. 7). Since 75 % of all measured Tn concentrations during the campaign were below $255\,Bq\,m^{-3}$, we consider the sbs result as representative for the systematic error of the Tn measurements. The manufacturer provided an Rn error of 2 % on the calibration certificates. The application of the bivariate regression analysis on the sbs data resulted in a systematic error for Rn in the range of 1 % to 6 %, which was corrected for.

The field measurements were conducted under partly harsh field conditions including changing temperatures and RHs for an extended period of two month, which is quite different to standard applications of the RAD7. Consequently, a careful and rigorous determination of the Tn random concentration error under field conditions was crucial to provide a basis for estimating the overall transport time uncertainty. The obtained

median random concentration error (precision) of the RAD7s for three concentration classes ($> 100\,\mathrm{Bq\,m^{-3}}$, 100–$15\,\mathrm{Bq\,m^{-3}}$, $< 15\,\mathrm{Bq\,m^{-3}}$) were 8.8 %, 23.2 % and 132.1 % for Tn and 16.6 %, 25.0 %, 99.2 % for Rn, respectively. The monitors proved to be suitable under all conditions at our field site to resolve vertical concentrations differences of Tn and also those of Rn under stable nighttime conditions. These findings, in combination with the comparably low prize and the Tn and Rn selectivity of the RAD7 may be convincing arguments for equipping a profile system with these monitors. However, it has to be kept in mind that the analyzer precision may not be sufficient for low Tn and Rn concentrations.

4.2 Comparison of transport times with existing empirical parameterizations

A comparison of our transport times with those of Lehmann et al. (1999) and Nemitz et al. (2009) revealed a reasonable agreement for the lowest layer (0.04–0.2 m), although the canopy structure was probably quite different for all study sites. In addition, we compared our measured and quality controlled transport times with currently existing parameterizations that are used in models such as SURFATM (see Personne et al., 2009). The transport time is expressed as the total resistance multiplied with the layer thickness (h).

$$\tau(\mathrm{surfatm}) = (R_{ac} + R_a(z_{ref})) \cdot h \tag{5}$$

where R_{ac} is the in-canopy and R_a the aerodynamic resistance (Thom, 1975) at the reference height ($z_{ref} = 0.8\,\mathrm{m}$). We calculated $\tau(\mathrm{surfatm})$ exemplarily for our overall layer (z_1–z_3) and for data from block 3 according to Personne et al. (2009) (equations modified):

$$R_{ac} = \frac{h_c \cdot \exp(\alpha_u)}{\alpha_u \cdot K_m(h_c)} \cdot \left\{ \exp\left(\frac{-\alpha_u \cdot z_{0s}}{h_c}\right) - \exp\left(\frac{\alpha_u \cdot (d + z_0)}{h_c}\right) \right\} \tag{6}$$

$$R_a(z_{ref}) = \frac{1}{\kappa^2 \cdot u(z_{ref})} \cdot \left\{ \ln\left[\frac{Z}{z_0}\right] - \Psi_H(Z/L) \right\} \cdot \left\{ \ln\left[\frac{Z}{z_0}\right] - \Psi_M(Z/L) \right\} \tag{7}$$

h_c is the canopy height, α_u the attenuation coefficient for the decrease of the wind speed inside the plant cover, z_{0s} the ground surface roughness length, d the displacement height, z_0 the canopy roughness height, K_m the eddy diffusivity coefficient ($K_m(h_c) = \kappa \cdot u_* \cdot (h_c - d)$), at h_c, κ the von-Kàrmàn constant, $u(z_{ref})$ the horizontal wind speed at z_{ref}, $Z = z_{ref} - d$, L the Monin-Obukhov length and Ψ_H and Ψ_M are the stability correction functions for heat and momentum, respectively. Furthermore, we compared our transport times with an empirical approach provided by van Pul and Jacobs (1994) used e.g. in the STOCHEM model (Sanderson et al., 2003), where the transport time is expressed as:

$$\tau(\text{vanPul}) = \left(\frac{13.9 \cdot \text{LAI} \cdot h_c^2}{u_*} \right) \tag{8}$$

where LAI is the single sided leaf area index. For our study, the LAI was 4.8 as determined by canopy harvest close to the inlets after the experiment.

Measured median transport times (τ) between z_1 and z_3 for all data from block 3 range between 350 s during nighttime to 220–290 s during daytime (Fig. 10). The values are in very good agreement with $\tau(\text{surfatm})$ during daytime from around 09:00 to 18:00 LT. However, nighttime values of $\tau(\text{surfatm})$ are significantly higher than the measured τ values and range between 700 s and 900 s. Although the transport in the layer just above the canopy is expressed by R_a, the value of $\tau(\text{surfatm})$ mainly depends on R_{ac} since the contribution of R_a is lower than 3 % at any time of the day. This reveals that the parameterization of R_{ac} by Personne et al. (2009) is not suitable to accurately calculate the in-canopy transport times during nighttime in this canopy. The reason for the much lower measured nighttime values of τ is the presence of unstable conditions and convective transport in the lowest part of the canopy, which was confirmed by measured temperature profiles (not shown). In contrast, $\tau(\text{vanPul})$ compares well with the measured τ values during nighttime, but is significantly lower during daytime with values of around 100 s. Since both parameterisations require u_* as input, which typically features very high uncertainties during prevailing low wind speeds (mainly at

nighttime), the contrasting results are remarkable. In addition, the Tn method showed a much smaller scatter than transport times derived from empirical parameterizations, as indicated by the inter-quartile range in Fig. 10.

4.3 Transport time uncertainty

Since during our experiment transport times of good quality and those of inadequate quality with high uncertainties were present, we conducted a detailed analysis to identify the inlet height arrangement with the optimal performance for the determination of transport times using the Tn method. We further investigated the dependencies of the transport time uncertainties (σ_τ). The comparison of the τ values of inadequate quality with the measured Tn concentration profiles (Fig. 8) indicates that inadequate quality may occur when (a) the concentration differences are very small (e.g. Fig. 8a and Fig. 9c; z_2 and z_3), or (b) the Tn concentration at the upper of both inlet heights (z_u) is very low (see Figs. 8b, 9d).

To investigate (a), we plotted the σ_τ values as a function of the measured Tn gradient for the entire Tn profile data set (51 days) including all inlet height arrangements (block 1–3) and heights (z_1, z_2, z_3), and found a strong exponential relationship (Fig. 11). Obviously, at high absolute gradients the uncertainty of the transport time is lowest and the uncertainty increases significantly with decreasing gradients. In order to obtain reliable values for the transport times with a relative $\frac{\sigma_\tau}{\tau}$ of < 0.5 an absolute gradient of at least $1000\,\mathrm{Bq\,m^{-3}\,m^{-1}}$ is desirable. In the intermediate Tn gradient range between 1000 and $350\,\mathrm{Bq\,m^{-3}\,m^{-1}}$ the values of $\frac{\sigma_\tau}{\tau}$ range from 0.3 to 0.6. For τ values with $\frac{\sigma_\tau}{\tau}$ smaller than unity the gradient should not be $< 70\,\mathrm{Bq\,m^{-3}\,m^{-1}}$. Using the findings from Fig. 11 we are able to deduce a minimal Tn concentration difference that has to be measured between two inlet heights in order to determine transport times of good quality. For example during period 1 between z_1 and z_2 (0.04 m and 0.1 m) this value is $60\,\mathrm{Bq\,m^{-3}}$, which is prevailing at any time. Additionally, the dependency of $\frac{\sigma_\tau}{\tau}$ on the Tn gradient underlines the importance of a careful choice of the inlet heights.

Of all determined τ values (block 1–3, z_1, z_2, z_3), 44 % are of good quality (pie diagram in Fig. 11), followed by 34 % and 22 % in the adequate and inadequate quality class, respectively. The data quality of the τ values presented for period 1 and 2 (pie diagrams in Fig. 9) is generally higher than the overall data quality, except for the upper layer during period 2 (Fig. 9d). Period 2 represents the inlet height arrangement during block 3 (Fig. 3), which is the longest of the three blocks. Hence, the quality of block 3 data dominates and lowers the overall data quality mainly due to the low data quality in the upper layer. This can be explained by (b) the influence of the measured Tn concentration at the upper inlet height ($C_{\mathrm{Tn}_{z_u}}$) in Eq. (1) on σ_τ, which we compare with the effect of the Tn concentration at the lower inlet height ($C_{\mathrm{Tn}_{z_l}}$) on σ_τ (exemplarily shown using the values measured at z_2 and z_1; Fig. 12). While the values of $C_{\mathrm{Tn}_{z_u}}$ were found to have a strong influence on the magnitude of σ_t (following a power function), the values of $C_{\mathrm{Tn}_{z_l}}$ showed only a weak impact. Higher values of $C_{\mathrm{Tn}_{z_u}}$ result in low absolute σ_τ values and lower $C_{\mathrm{Tn}_{z_u}}$ values cause a substantial increase of σ_τ. Since the soil is the Tn source and z_u is located more far away from the ground than z_l, lower Tn concentrations are expected to be measured at z_u. This fact automatically increases the probability that $C_{\mathrm{Tn}_{z_u}}$ is close to or below the LOD, where the relative value of $\sigma C_{\mathrm{Tn}_{z_u}}$ can be close to or even higher than unity. Since $\sigma C_{\mathrm{Tn}_{z_u}}$ is propagated it may cause very high values of σ_τ. Furthermore, $C_{\mathrm{Tn}_{z_u}}$ is the denominator in Eq. (1) and thus strongly impacts τ. Consequently, a more compact vertical inlet height separation will provide more reliable τ values. The vertical limit of the inlet height separation for our system at any site can be assessed by applying the results in Fig. 11.

4.4 Contribution of individual error propagation terms

We additionally quantified the contribution of the individual error propagation terms A, B and C (Eq. 4) to the total transport time uncertainty σ_t. Note that the sum of error terms A and B can be reduced by term C (cf. Eq. 4). Figure 13 presents the error partitioning

as a function of the $C_{\mathrm{Tn}_{z_l}}/C_{\mathrm{Tn}_{z_u}}$ ratio for our entire Tn dataset. Generally, terms A and B contribute with up to 50 % and 50–100 % to the overall uncertainty σ_t, respectively. This highlights the strong impact of $C_{\mathrm{Tn}_{z_u}}$ on σ_t. Term A shows a tendency to shift from 0 % to 50 % with a decreasing Tn concentration ratio $C_{\mathrm{Tn}_{z_l}}/C_{\mathrm{Tn}_{z_u}}$ (Fig. 13). For exam-
5 ple, during periods with $C_{\mathrm{Tn}_{z_l}}/C_{\mathrm{Tn}_{z_u}}$ ratios below 2.5 the terms A and B contribute to the total uncertainty with about 30–50 % and 70–50 %, respectively. In contrast, under conditions when the $C_{\mathrm{Tn}_{z_l}}/C_{\mathrm{Tn}_{z_u}}$ ratio is higher than 2.5, term B can account for up to 100 % to the total uncertainty. We found that term C can reduce the sum of term A and B by 0–43 % for our dataset (not shown), and strongly depends on the correlation coefficient
10 $r_{(C_{\mathrm{Tn}_{z_l}}, C_{\mathrm{Tn}_{z_u}})}$ of the measured Tn concentrations at the two heights.

5 Summary and conclusions

We present and characterize a novel automated system for the measurement of vertical Tn and Rn profiles near the ground. In contrast to most previous studies, we perform continuous measurements with one single instrument per inlet height using
15 commercially available monitors (RAD7) that are selective for Tn and Rn. Hence, the major progress of the system is its suitability for the direct determination of the in-canopy transport time from vertical Tn concentration differences. We found that the system, including optimized chambers, alpha detectors and flows, is suitable to detect vertical differences of Tn and also those of Rn close to a relatively strong source
20 (e.g. in low canopies). The performance of the system was investigated by considering (a) residence times of the air in the system, including the effect of filter clogging, (b) validation of the Tn sensitivity using a primary standard, (c) determination of the limits of detection, and (d) a rigorous determination of systematic and random errors for Tn concentrations measured under field conditions. These achievements were the
25 prerequisite to analyze the inlet height arrangements required to obtain a high data quality. The system was operated during an intensive field campaign for two month

at a natural grassland ecosystem. Vertical concentration profiles of Tn and Rn for two periods with different inlet height arrangements are presented. For the first time, we calculate transport times (τ) directly from selectively measured Tn concentration profiles and propagate the uncertainty of the in-canopy transport time (σ_τ) from the random Tn concentration errors (σC_{Tn}). The averaged σC for Tn and Rn was determined to be $\sigma C_{Tn} = \frac{0.10C + 13.2\,\mathrm{Bq\,m^{-3}}}{\sqrt{2}}$ and $\sigma C_{Rn} = \frac{0.19C + 9.5\,\mathrm{Bq\,m^{-3}}}{\sqrt{2}}$. A quality assessment of the transport times revealed a good data quality with relative uncertainties below 50 % for 44 % of all determined transport times during the field experiment. The occasional occurrence of transport time uncertainties higher than 100 % are related to measured absolute Tn gradients below $70\,\mathrm{Bq\,m^{-3}\,m^{-1}}$ and occur for 22 % of all calculated transport times. Large gradients cause smaller relative transport time errors. In addition, the method appears highly sensitive to the Tn concentration measured in the upper height ($C_{Tn_{z_u}}$). Low values of $C_{Tn_{z_u}}$ result in high absolute values of σ_τ. An analysis of the contribution of individual error propagation terms to σ_τ underlines these findings. It should be noted that to obtain large gradients it is preferable to increase the vertical separation of the measurement heights as much as possible. For Rn, this is possible to some extend since $C_{Rn_{z_u}}$ decreases only as a result of dilution by turbulence. However, the vertical inlet separation is much more limited for the determination of the transport time by the fast Tn decay due to sharply decreasing values of C_{Tn} with height. Consequently, the analyser with the best precision should always be placed in the uppermost height, whose position has to be chosen very carefully. The major requirement for the future is the improvement of the RAD7 precision at low concentrations, which implies a decrease of the LOD. This might be achieved by further increasing the size of the measurement chamber as well as the active surface area of the alpha detectors.

Our setup allows the quantification of τ within the grass canopy for different layers. The transport times may subsequently be converted into a vertical profile of bulk diffusion coefficients. Our results provide an excellent basis for a reliable investigation of turbulence-chemistry interactions (e.g. Damköhler number) in canopies. The

uncertainties of τ values determined with the Tn or Rn method should be considered for the interpretation of results in further studies.

References

Brost, R. A. and Chatfield, R. B.: Transport of radon in a 3-Dimensional, subhemispheric model, J. Geophys. Res.-Atmos., 94, 5095–5119, doi:10.1029/Jd094id04p05095, 1989.

Butterweck, G., Reineking, A., Kesten, J., and Porstendorfer, J.: The use of the natural radioactive noble-gases radon and thoron as tracers for the study of turbulent exchange in the atmospheric boundary-layer – case-study in and above a wheat field, Atmos. Environ., 28, 1963–1969, 1994.

Cantrell, C. A.: Technical Note: Review of methods for linear least-squares fitting of data and application to atmospheric chemistry problems, Atmos. Chem. Phys., 8, 5477–5487, doi:10.5194/acp-8-5477-2008, 2008.

Currie, L. A.: Limits for qualitative detection and quantitative determination – application to radiochemistry, Anal. Chem., 40, 586–593, doi:10.1021/ac60259a007, 1968.

Dearellano, J., Duynkerke, P. G., and Builtjes, P. J. H.: The divergence of the turbulent-diffusion flux in the surface-layer due to chemical-reactions - the NO-O_3-NO_2 system, Tellus B, 45, 23–33, doi:10.1034/j.1600-0889.1993.00002.x, 1993.

Denmead, O. T. and Bradley, E. F.: Flux-gradient relationships in a forest canopy, in: The Forest-Atmosphere Interaction, edited by: Hutchinson, B. A. and Hicks, B. B., Reidel, Dordrecht, 421 pp., 1985.

Dlugi, R., Berger, M., Zelger, M., Hofzumahaus, A., Siese, M., Holland, F., Wisthaler, A., Grabmer, W., Hansel, A., Koppmann, R., Kramm, G., Möllmann-Coers, M., and Knaps, A.: Tur-

Title Page

Abstract	Introduction
Conclusions	References
Tables	Figures

| ◄ | ► |
| ◄ | ► |

Back | Close

Full Screen / Esc

Printer-friendly Version

Interactive Discussion

bulent exchange and segregation of HO_x radicals and volatile organic compounds above a deciduous forest, Atmos. Chem. Phys., 10, 6215–6235, doi:10.5194/acp-10-6215-2010, 2010.

Dorr, H., Kromer, B., Levin, I., Munnich, K. O., and Volpp, H. J.: CO_2 and radon 222 as tracers for atmospheric transport, J. Geophys. Res.-Oc. Atm., 88, 1309–1313, 1983.

Finnigan, J.: Turbulence in plant canopies, Annu. Rev. Fluid Mech., 32, 519–571, doi:10.1146/annurev.fluid.32.1.519, 2000.

Gut, A., Scheibe, M., Rottenberger, S., Rummel, U., Welling, M., Ammann, C., Kirkman, G. A., Kuhn, U., Meixner, F. X., Kesselmeier, J., Lehmann, B. E., Schmidt, W., Muller, E., and Piedade, M. T. F.: Exchange fluxes of NO_2 and O_3 at soil and leaf surfaces in an Amazonian rain forest, J. Geophys. Res.-Atmos., 107, LBA 27-1–LBA 27-15, doi:10.1029/2001JD000654, 2002.

Hänsel, H. and Neumann, W.: Physik, Spectrum, Akad. Verl., Heidelberg, Berlin, Oxford, 1995.

Hens, K.: Der bodennahe, vertikale, turbolente Transport von ^{222}Rn, ^{220}Rn und anderen Spurengasen im Stammraum eines Fichtenbestandes, Diplom, Institut für Physik, Johannes Gutenberg – Universität, Mainz, 93 pp., 2009 (in German).

Ikebe, Y. and Shimo, M.: Estimation of vertical turbulent diffusivity from thoron profiles, Tellus, 24, 29–37, doi:10.1111/j.2153-3490, 1972.

Israel, G. W.: Thoron (^{220}Rn) Measurements in the atmosphere and their application in meteorology, Tellus B, 17, 383–388, 1965.

Lehmann, B. E., Lehmann, M., Neftel, A., Gut, A., and Tarakanov, S. V.: Radon-220 calibration of near-surface turbulent gas transport, Geophys. Res. Lett., 26, 607–610, 1999.

Lide, D. R.: CRC Handbook of Chemistry and Physics: a Ready-Reference Book of Chemical and Physical Data, 85th Edn., CRC Press, Boca Raton, 2589 pp., 2004.

Liu, S. C., McAfee, J. R., and Cicerone, R. J.: Radon 222 and Tropospheric Vertical Transport, J. Geophys. Res., 89, 7291–7297, 1984.

Martens, C. S., Shay, T. J., Mendlovitz, H. P., Matross, D. M., Saleska, S. R., Wofsy, S. C., Woodward, W. S., Menton, M. C., De Moura, J. M. S., Crill, P. M., De Moraes, O. L. L., and Lima, R. L.: Radon fluxes in tropical forest ecosystems of Brazilian Amazonia: night-time CO_2 net ecosystem exchange derived from radon and eddy covariance methods, Glob. Change Biol., 10, 618–629, 2004.

Nemitz, E., Loubet, B., Lehmann, B. E., Cellier, P., Neftel, A., Jones, S. K., Hensen, A., Ihly, B., Tarakanov, S. V., and Sutton, M. A.: Turbulence characteristics in grassland canopies and im-

Title Page

Abstract | Introduction

Conclusions | References

Tables | Figures

◄ | ►|

◄ | ►

Back | Close

Full Screen / Esc

Printer-friendly Version

Interactive Discussion

plications for tracer transport, Biogeosciences, 6, 1519–1537, doi:10.5194/bg-6-1519-2009, 2009.

Pape, L., Ammann, C., Nyfeler-Brunner, A., Spirig, C., Hens, K., and Meixner, F. X.: An automated dynamic chamber system for surface exchange measurement of non-reactive and reactive trace gases of grassland ecosystems, Biogeosciences, 6, 405–429, doi:10.5194/bg-6-405-2009, 2009.

Personne, E., Loubet, B., Herrmann, B., Mattsson, M., Schjoerring, J. K., Nemitz, E., Sutton, M. A., and Cellier, P.: SURFATM-NH3: a model combining the surface energy balance and bi-directional exchanges of ammonia applied at the field scale, Biogeosciences, 6, 1371–1388, doi:10.5194/bg-6-1371-2009, 2009.

Rottger, A. and Honig, A.: Recent developments in radon metrology: new aspects in the calibration of radon, thoron and progeny devices, Radiat. Prot. Dos., 145, 260–266, doi:10.1093/Rpd/Ncr047, 2011.

Sanderson, M. G., Collins, W. J., Derwent, R. G., and Johnson, C. E.: Simulation of global hydrogen levels using a lagrangian three-dimensional model, J. Atmos. Chem., 46, 15–28, doi:10.1023/A:1024824223232, 2003.

Simon, E., Lehmann, B. E., Ammann, C., Ganzeveld, L., Rummel, U., Meixner, F. X., Nobre, A. D., Araujo, A., and Kesselmeier, J.: Lagrangian dispersion of Rn-222, H_2O and CO_2 within Amazonian rain forest, Agr. Forest Meteorol., 132, 286–304, 2005.

Staudt, K., Serafimovich, A., Siebicke, L., Pyles, R. D., and Falge, E.: Vertical structure of evapotranspiration at a forest site (a case study), Agr. Forest Meteorol., 151, 709–729, doi:10.1016/j.agrformet.2010.10.009, 2011.

Taylor, J. R.: An Introduction to Error Analysis. The Study of Unvertainties in Physical Measurements, University Science Books, Sausalito, California, 1997.

Thom, A. S.: Momentum, mass and heat exchange of plant communities, in: Vegetation and the Atmosphere, edited by: Monteith, J. L., Academic Press, London, 57–109, 1975.

Trumbore, S. E., Keller, M., Wofsy, S. C., and Dacosta, J. M.: Measurements of soil and canopy exchange-rates in the Amazon rain-forest using Rn-222, J. Geophys. Res.-Atmos., 95, 16865–16873, 1990.

Ussler, W., Chanton, J. P., Kelley, C. A., and Martens, C. S.: Radon-222 tracing of soil and forest canopy trace gas-exchange in an open canopy boreal forest, J. Geophys. Res.-Atmos., 99, 1953–1963, 1994.

Title Page

Abstract | Introduction

Conclusions | References

Tables | Figures

◄ | ►

◄ | ►

Back | Close

Full Screen / Esc

Printer-friendly Version

Interactive Discussion

van Pul, W. A. J. and Jacobs, A. F. G.: The conductance of a maize crop and the underlying soil to ozone under various environmental-conditions, Bound.-Lay. Meteorol., 69, 83–99, 1994.

Wada, A., Murayama, S., Kondo, H., Matsueda, H., Sawa, Y., and Tsuboi, K.: Development of a compact and sensitive electrostatic radon-222 measuring system for use in atmospheric observation, J. Meteorol. Soc. Jpn., 88, 123–134, doi:10.2151/jmsj.2010-202, 2010.

Wicke, A. and Porstendorfer, J.: Application of surface barrier detectors for the measurement of environmental radon and radon daughters in air, International Meeting on Radon-Radon Progeny Measurements, Washington DC, September 1983, 1983.

Wolff, V., Trebs, I., Ammann, C., and Meixner, F. X.: Aerodynamic gradient measurements of the NH_3-HNO_3-NH_4NO_3 triad using a wet chemical instrument: an analysis of precision requirements and flux errors, Atmos. Meas. Tech., 3, 187–208, doi:10.5194/amt-3-187-2010, 2010.

Yienger, J. J. and Levy, H.: Empirical-Model of Global Soil-Biogenic NO_x Emissions, J. Geophys. Res.-Atmos., 100, 11447–11464, doi:10.1029/95jd00370, 1995.

Zahorowski, W., Chambers, S. D., and Henderson-Sellers, A.: Ground based radon-222 observations and their application to atmospheric studies, J. Environ. Radioactiv., 76, 3–33, 2004.

Zhang, K., Wan, H., Zhang, M., and Wang, B.: Evaluation of the atmospheric transport in a GCM using radon measurements: sensitivity to cumulus convection parameterization, Atmos. Chem. Phys., 8, 2811–2832, doi:10.5194/acp-8-2811-2008, 2008.

Title Page

Abstract | Introduction

Conclusions | References

Tables | Figures

◄ | ►►

◄ | ►

Back | Close

Full Screen / Esc

Printer-friendly Version

Interactive Discussion

Table 1. Details of the hardware components used for the automated Tn and Rn profile system.

Part	Manufacturer	Specifications
inline filter case	Entegris Inc., USA	Galtek Integral Ferrule in-line filters
membrane filter	Pall Corporation, USA	Zyklon membrane disc filters, model P4PH047, pore size 5 μm, diameter 47 mm
PFA tubing	Saint-Gobain Performance Plastics Isoflour GmbH, Germany	inner diameter (ID) 4 mm, outer diameter 6.35 mm
tube heating	AEG Haustechnik, Germany	heating wire, type SLH 15
pressure sensor	Sensor Technics, Germany	600–1100 hPa type HDI0611ARY8P5
sample pump	KNF Neuberger, Germany	membrane pump, type DCB24V N86KTDCB
Nafion dryer	Perma Pure, USA	length 3.55 m, ID 2.18 mm, type PPMD-110-144F
MFC	Vögtlin, Switzerland	range 0.05–5 L min^{-1}, precision 0.3 %, type Red-y smart controller GSC-B hi-performance
RAD7	Durridge, USA	Tn and Rn monitor, range Rn: 4–400 000 Bq m^{-3}
drying pump	Gardner Denver, Thomas Subdivision, USA	type: 607CD22
needle valve	Kurt J. Lesker Company, USA	type: Nupro SS-SS4

An automated system for selective and continuous measurements

D. Plake and I. Trebs

Table 2. Limits of detection (LOD in $Bq\,m^{-3}$) of the RAD7 monitors (with the system characteristics described in Sect. 2.2) determined under field conditions during the zero air measurements.

RAD7	$LOD_{\textbf{Tn}}$	mean LOD_{Tn}	LOD_{Rn}	mean LOD_{Rn}
z_1	18.1		5.8	
z_2	22.0	18.3	6.4	6.2
z_3	14.7		6.4	
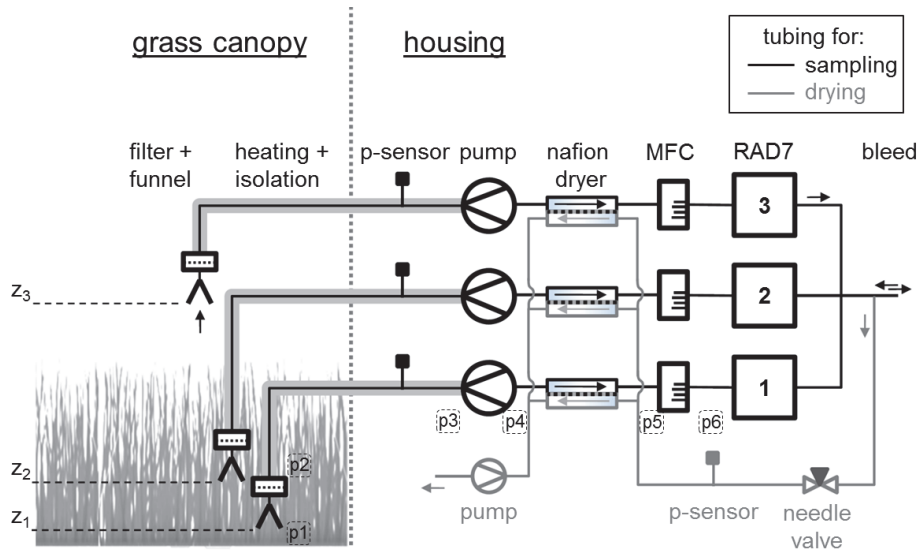
Fig. 1. Simplified gas flow scheme of the automated Tn and Rn profile system. The positions of the pressure measurements ($p1$–$p6$) mentioned in Sect. 2.4.1 are indicated.
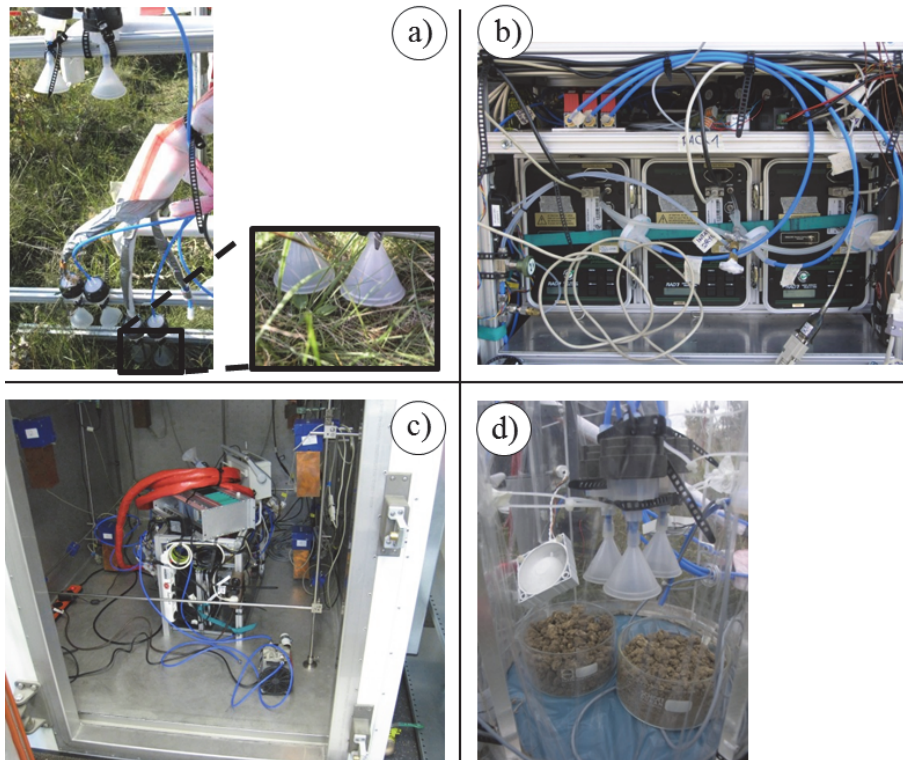
Fig. 2. Setup of the automated Tn and Rn profile system: **(a)** field installation of the inlets, **(b)** rack installation of the system in the housing, **(c)** setup in the thoron progeny chamber of the PTB in Braunschweig, **(d)** arrangement of inlets and soil samples during the side-by-side measurements in the dynamic chamber.

D. Plake and I. Trebs
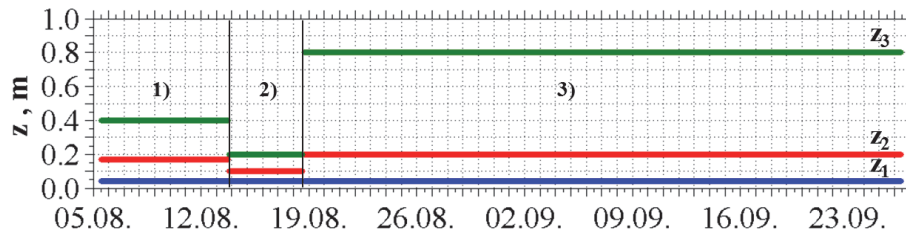
Fig. 3. Arrangement of the inlet heights (z_1–z_3) for the automated Tn and Rn profile measurements. The measurement campaign was divided into three blocks: (1) 5–13 August: $z_1 = 0.04$, $z_2 = 0.17$, $z_3 = 0.40$ m; (2) 13–18 August: $z_1 = 0.04$, $z_2 = 0.1$ m, $z_2 = 0.20$ m; (3) 18 August–26 September: $z_1 = 0.04$, $z_2 = 0.20$, $z_3 = 0.80$ m.
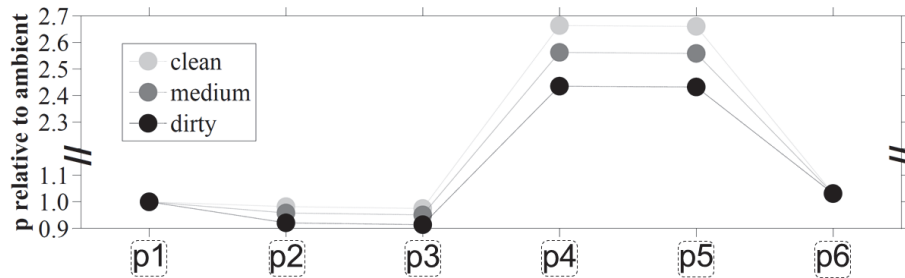
Fig. 4. Pressures measured at positions $p1$–$p6$ within the automated Tn and Rn profile system ($p1$ = ambient pressure) during the filter clogging simulation (clean, medium, dirty).
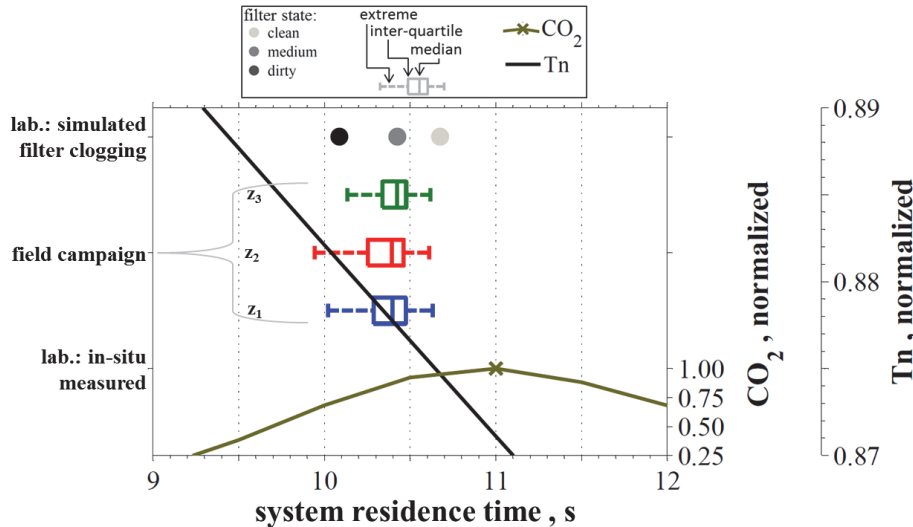
Fig. 5. Comparison of (i) calculated residence times from the simulated filter clogging experiment in the laboratory (filled circles), (ii) residence times determined from the field data set (z_1–z_3 with median, inter-quartile range and extreme values) and (iii) in-situ measured residence times (CO_2 experiment, green line) with (iv) the resulting radioactive Tn decay (black line) calculated from Eq. (1).
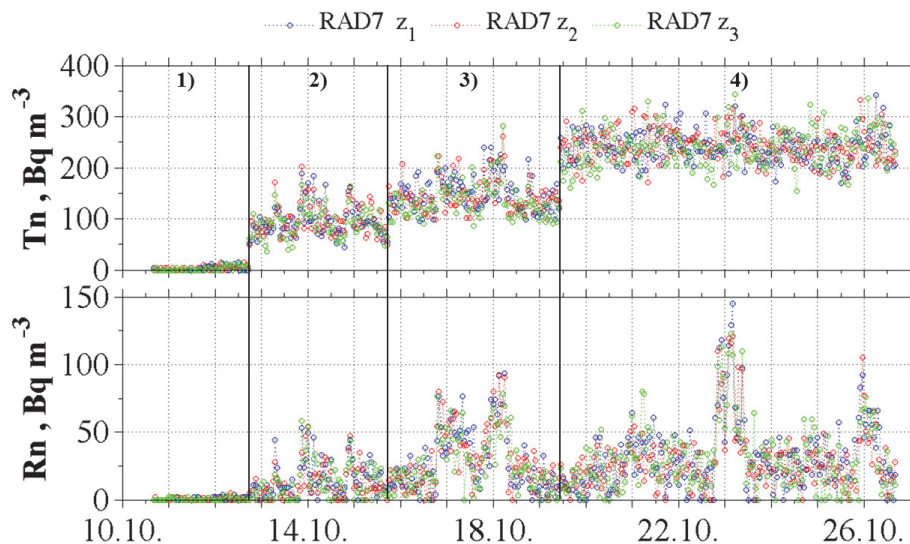
Fig. 6. Time series of Tn and Rn concentrations during sixteen days of side-by-side measurements (10–26 October 2011) measured with the RAD7 monitors (60 min integration time). After the zero air measurement (1) we purged the chamber with $70\,L\,min^{-1}$ (2), $35\,L\,min^{-1}$ (3), and $5\,L\,min^{-1}$ (4).
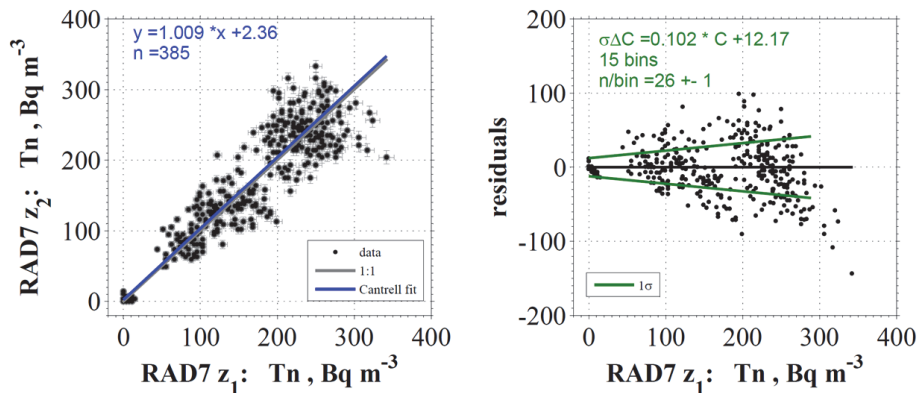
Fig. 7. Example of systematic and random error determination from side-by-side measurements. Left panel: determination of the systematic error of the Tn concentration between the RAD7 at z_1 and z_2 using the bivariate weighted linear least-squares fitting regression analysis by the Williamson-York method (Cantrell, 2008). Error bars represent the uncertainties from counting statistics of the RAD7 ($\sigma = \sqrt{n}$). Right panel: quantification of the random error ($\sigma\Delta C$) using the 1σ scatter of the residuals around the fit (for details see Sect. 2.5 and Wolff et al., 2010a).
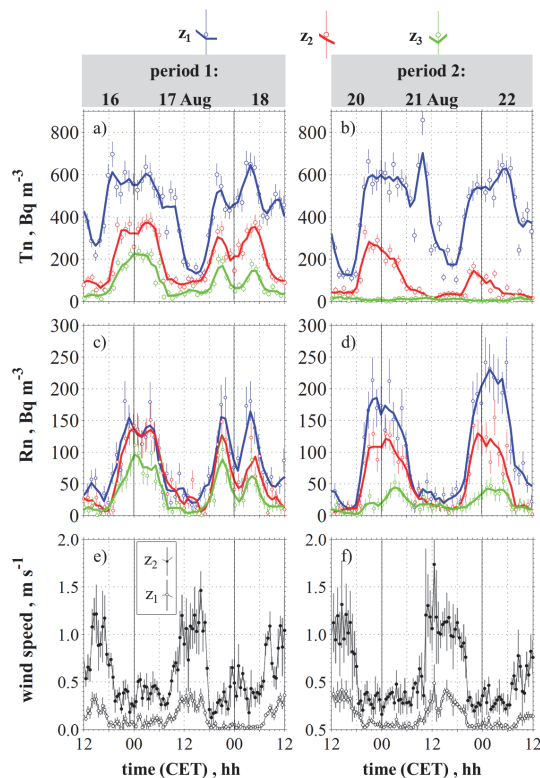
Fig. 8. Tn and Rn concentrations as well as wind speeds (z_1 = 0.2 m, z_2 = 0.8 m) measured during two periods with different inlet height arrangements (period 1: 16–18 August, period 2: 20–22 August, see Fig. 3). Dots with error bars in plots **(a)**–**(d)** represent the RAD7 concentration readings (integration time 60 min) and the corresponding random errors (σC). The solid lines show the running means (width: 3 h) of the concentrations. In plots **(e)** and **(f)** 30 min averages of the measured wind speed are shown, where error bars represent standard deviations.
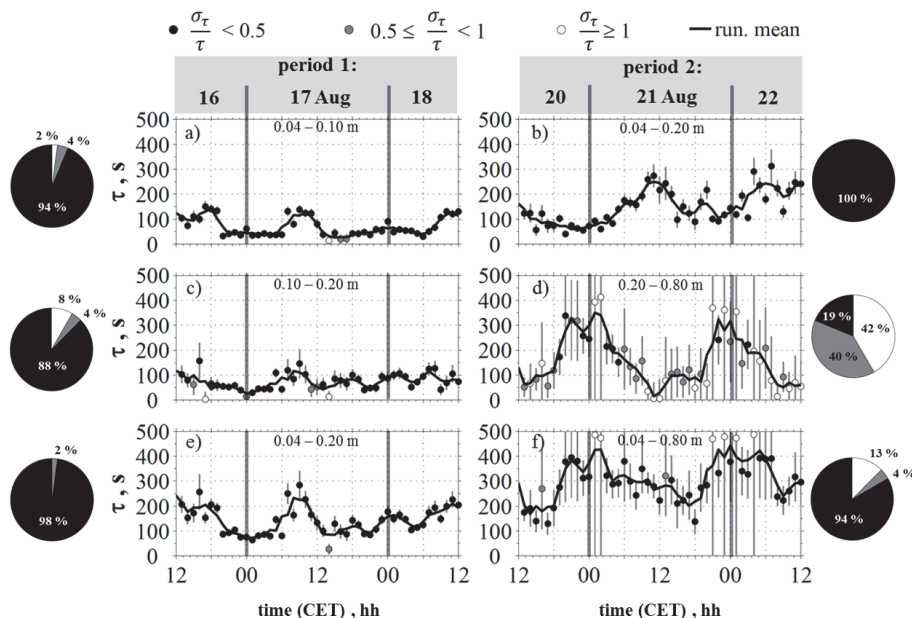
Fig. 9. Calculated transport times τ for three layers (lower (**a** and **b**), upper (**c** and **d**), and overall (**e** and **f**)) classified according to the magnitude of the relative uncertainty for the two selected periods. The error bars represent the absolute uncertainty of τ determined using Gaussian error propagation (Eq. 4). The pie diagrams represent the percentage of τ in each quality class for the plots shown (black: good, grey: adequate, white: inadequate quality).

Title Page

Abstract | Introduction

Conclusions | References

Tables | Figures

◄ | ►

◄ | ►

Back | Close

Full Screen / Esc

Printer-friendly Version

Interactive Discussion
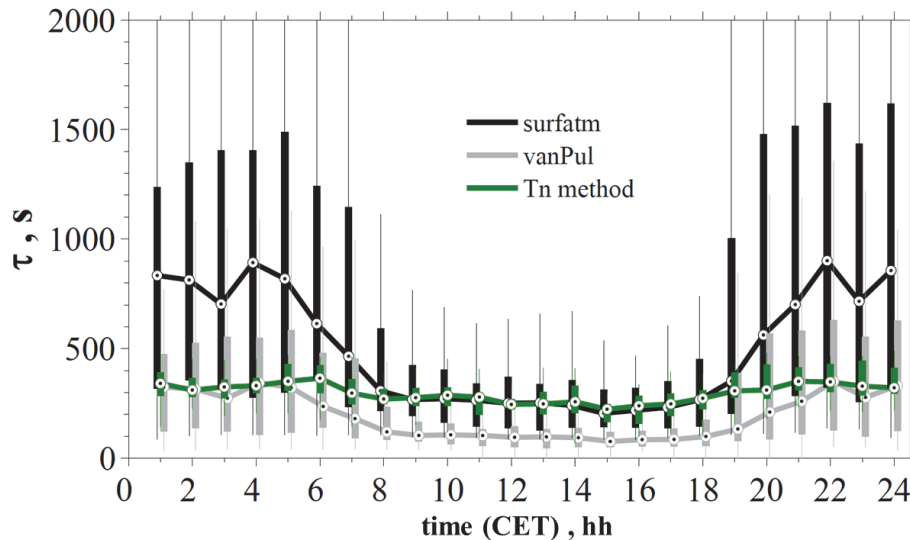
Fig. 10. Median diurnal course of measured transport times between 0.04 and 0.8 m using the Tn method (values of inadequate quality were rejected) compared to existing empirical parameterisations from the literature for all data from block 3 for the natural grassland site. The statistical distribution of the data sets is represented by hourly boxplots. The dots indicate the medians, the filled boxes cover the inter-quartile range and the whiskers represent the extreme data points.
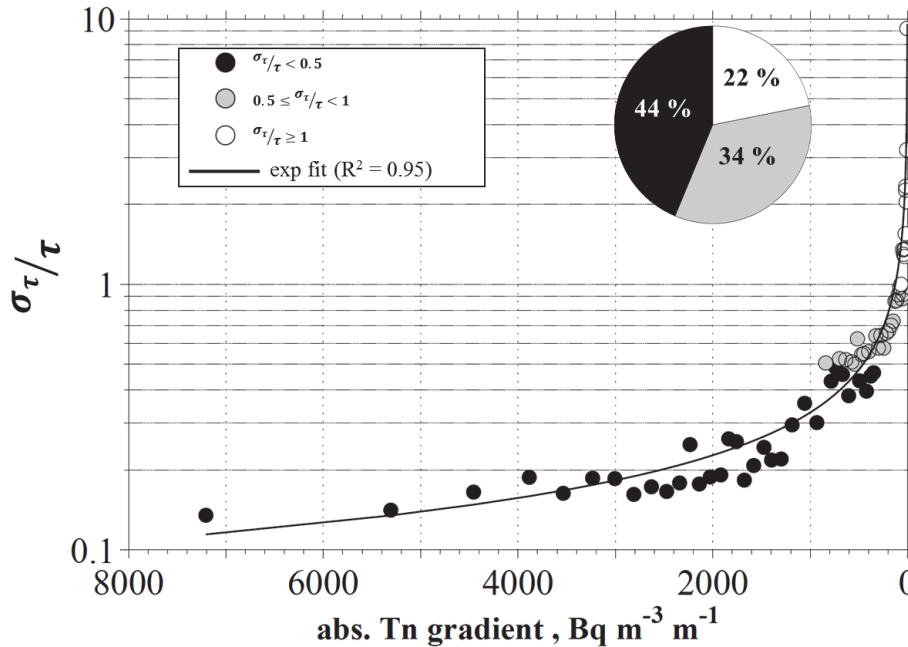
Fig. 11. Dependency of the relative uncertainty of the transport time ($\frac{\sigma_\tau}{\tau}$) on the absolute prevailing Tn gradient for the entire Tn profile data set (51 days) including all inlet height arrangements (block 1–3) and heights (z_1, z_2, z_3). The data were sorted by the magnitude of the Tn gradient and averages of bins ($n = 50$) were calculated before the exponential fit was made. The pie diagram summarises the fraction of τ values in each quality class (black: good, grey: adequate, white: inadequate quality, see text for details).
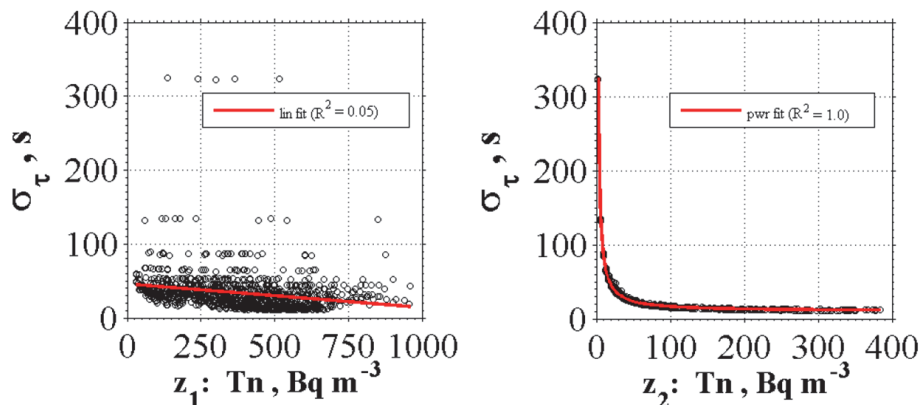
Fig. 12. Dependency of the absolute uncertainty of the transport time (σ_t) on the Tn concentrations measured at the upper ($C_{Tn_{z_u}}$) and lower ($C_{Tn_{z_l}}$) inlet positions using the data from z_1 (left panel) and z_2 (right panel) for the entire data set (51 days) including all inlet height arrangements (block 1–3).
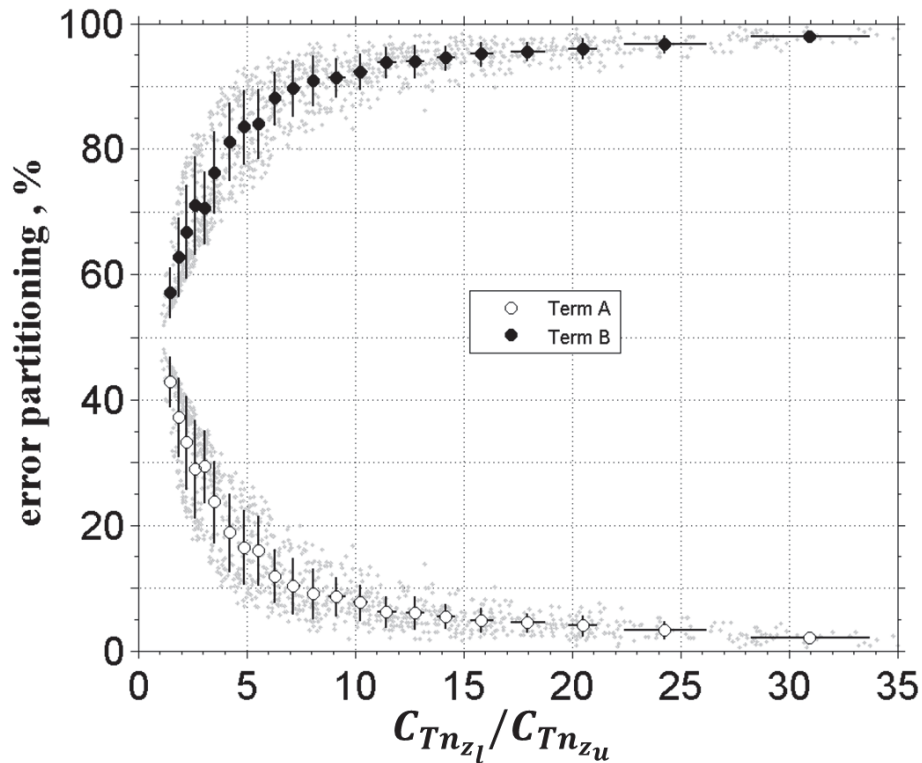
Fig. 13. The error partitioning of Term A and B in Eq. (4) as a function of the $C_{Tn_{z_l}}/C_{Tn_{z_u}}$ ratio for the entire data set (51 days) including all inlet height arrangements (block 1–3) and heights (z_1, z_2, z_3).